THE JOURNAL OF BIOLOGICAL CHEMISTRY VOL. 291, NO. 27, pp. 14248–14256, July 1, 2016

Rifampin Resistance Mutations Are Associated with Broad Chemical Remodeling of *Mycobacterium tuberculosis*[*] [S]

Received for publication, February 2, 2016, and in revised form, April 15, 2016 Published, JBC Papers in Press, May 10, 2016, DOI 10.1074/jbc.M116.716704

Nivedita Lahiri[‡], Rupal R. Shah[§], Emilie Layre[‡], David Young[‡], Chris Ford[§], Megan B. Murray[¶], Sarah M. Fortune[§], and D. Branch Moody[‡1]

From the [‡]Division of Rheumatology, Immunology, and Allergy, Brigham and Women's Hospital and Harvard Medical School, Boston, Massachusetts 02115 and the Departments of [§]Immunology and Infectious Diseases and [¶]Epidemiology, Harvard T. H. Chan School of Public Health, Boston, Massachusetts 02115

Global control of tuberculosis has become increasingly complicated with the emergence of multidrug-resistant strains of *Mycobacterium tuberculosis*. First-line treatments are anchored by two antibiotics, rifampin and isoniazid. Most rifampin resistance occurs through the acquisition of missense mutations in the rifampin resistance-determining region, an 81-base pair region encoding the rifampin binding site on the β subunit of RNA polymerase (*rpoB*). Although these mutations confer a survival advantage in the presence of rifampin, they may alter the normal process of transcription, thereby imposing significant fitness costs. Because the downstream biochemical consequences of the *rpoB* mutations are unknown, we used an organism-wide screen to identify the number and types of lipids changed after *rpoB* mutation. A new mass spectrometry-based profiling platform systematically compared ~10,000 cell wall lipids in a panel of rifampin-resistant mutants within two genetically distinct strains, CDC1551and W-Beijing. This unbiased lipidomic survey detected quantitative alterations (>2-fold, $p < 0.05$) in more than 100 lipids in each mutant. By focusing on molecular events that change among most mutants and in both genetic backgrounds, we found that rifampin resistance mutations lead to altered concentrations of mycobactin siderophores and acylated sulfoglycolipids. These findings validate a new organism-wide lipidomic analysis platform for drug-resistant mycobacteria and provide direct evidence for characteristic remodeling of cell wall lipids in rifampin-resistant strains of *M. tuberculosis*. The specific links between rifampin resistance and named lipid factors provide diagnostic and therapeutic targets that may be exploited to address the problem of drug resistance.

Mycobacterium tuberculosis remains a leading cause of death worldwide from an infectious disease (1). The emergence of highly drug-resistant organisms has complicated efforts to control the global tuberculosis epidemic (2). First-line tuberculosis treatment involves four drugs, the two most effective of which are isoniazid and rifampin. Strains resistant to rifampin alone, although once considered rare, now make up a large percentage of monoresistant *M. tuberculosis* isolates (3, 4). Moreover, resistance to both rifampin and isoniazid constitutes a clinical state of multidrug resistance, which necessitates treatment with a complicated second-line regimen that is both more toxic and less effective than standard chemotherapy (5). However, when identified, multidrug-resistant bacteria can be treated (5). Multidrug resistance is also a necessary intermediate in the evolution of even more highly resistant forms of *M. tuberculosis*, including those resistant to most or all available agents.

Rifampin resistance is conferred by mutation of its target, the β subunit of the RNA polymerase (RpoB).[2] In *M. tuberculosis*, most of the rifampin resistance in clinical isolates stems from amino acid changes at positions 513, 522, 526, and 531 of RpoB, which are near the rifampin binding site. Mutations at positions 531 and 526 are by far the most common and tend to show higher-level resistance (6, 7). The high correspondence between RpoB mutations and phenotypic rifampin resistance forms the basis of the now widely used "gene expert test," in which rapid detection of *rpoB* mutation effectively bypasses the need for cumbersome *in vitro* culture methods in many situations (8). The discrepancy between the number of *rpoB* mutations observed clinically and *in vitro* suggests that many *rpoB* mutations confer a significant fitness cost *in v*ivo. Supporting this idea, secondary mutations have been observed in patients (9). Thus, genetic mutation of this target is a common upstream event in rifampin resistance generation. Therefore, a more detailed understanding of the consequences of *rpoB* mutation could potentially provide diagnostic targets and a physiological understanding of mycobacterial adaptation to rifampin resistance as a core part of the multidrug resistance phenotype.

The mechanism by which *rpoB* mutations cause rifampicin resistance has been inferred from classic experiments in *Escherichia coli* that showed that specific rifampin resistance causing *rpoB* mutations altered aspects of transcription (10, 11). Transcriptomic analysis of *M. tuberculosis* after rpoB mutation likewise demonstrates durable transcriptional change in this species (12, 13). However, the specific downstream conse-

* This work was supported by National Institutes of Health Grants U19 AI076217, U19 AI111224, R01 AI049313, and P30 AI060354 and the Burroughs Wellcome Foundation. The authors declare that they have no conflicts of interest with the contents of this article. The content is solely the responsibility of the authors and does not necessarily represent the official views of the National Institutes of Health.

[S] This article contains supplemental Figs. S1–S5.

[1] To whom correspondence should be addressed: Division of Rheumatology, Immunology, and Allergy, Brigham and Women's Hospital and Harvard Medical School, Smith Bldg., Rm. 514, 1 Jimmy Fund Way, Boston, MA 02115. E-mail: bmoody@rics.bwh.harvard.edu.

[2] The abbreviations used are: RpoB, RNA polymerase B; PDIM, phthiocerol dimycocerosate; SGL, sulfoglycolipid; ESI, electrospray ionization mass spectrometry.

quences of an altered transcription apparatus on cell physiology, metabolism, and function are less clear. Transcriptional profiling of rifampin-resistant *M. tuberculosis* demonstrates changes in the expression of genes encoding secreted proteins, and proteomic profiling demonstrates alterations in some enzymes and lipid biosynthetic intermediates in the phthiocerol dimycocerosate (PDIM) pathway (12, 13). However, the extent to which rifampin resistance alters PDIM structures or concentrations or controls remodeling of other biochemical components of the multilayered cell wall remains unknown. Cell wall lipids, particularly cell surface polyketides, interface directly with the host and regulate immunogens that are exposed to the host (14) and have been known to control the permeability of the organism (15–18) in ways that might affect the transport of other drugs. Also, if these candidate cell wall changes can be reproducibly associated with drug resistance phenotypes, then altered lipids might also function as biochemical markers of the drug-resistant state (19).

Here we hypothesized that characteristic biochemical changes might occur with the acquisition of rifampin resistance in *M. tuberculosis*. Unlike other antibiotics that target specific chemical targets, such as enzymes that produce mycolic acid or peptidoglycan, the altered RpoB-dependent transcriptional apparatus would be expected to affect nearly any enzyme or regulator of lipid synthesis (7). Because there is no rational way to predict which lipids might be changed, we considered that an unbiased, organism-wide biochemical profiling approach would be most useful. Such analyses are now feasible as a result of the validation of comparative lipidomics platforms that use normal-phase HPLC-MS for separating and rapidly scanning many thousands of lipids in a single experiment (20–23). Using accurate mass retention time values as addresses, we can align all lipids present in both drug-resistant and drug-sensitive bacteria and generate thousands of intensity ratios for each aligned pair, providing an organism-wide screen for lipids altered in concentration after acquisition of rifampin resistance. This new method of comparative lipidomics can selectively identify any lipid changed in intensity with low rates (<1%) of false positive discovery (20, 21, 23). By applying these tools to a panel of isogenic *rpoB* mutants that represent both common and rare genetic changes seen in patient isolates, we sought to identify the scope of bacterial cell wall changes and identify the particular molecules common to all *M. tuberculosis* strains that have acquired rifampin resistance.

Experimental Procedures

Bacterial Strains, Medium, and Reagents—CDC1551 and W-Beijing mycobacterial strains were cultivated in Middlebrook 7H9 broth medium supplemented with oleic acid-albumin-dextrose-catalase, 0.05% Tween 80, and 0.5% glycerol for growth assays, to generate resistance mutants, and to count bacteria. Subsequently, Tween-free medium was used to generate samples for mass spectrometry analysis. Rifampin-resistant strains were selected in the presence of rifampin at a concentration of 2 μg/ml as published previously (24). Resistant colonies were picked and cultured in the absence of rifampin for subsequent analysis. All *rpoB* mutations were defined by Sanger sequencing of *rpoB* as published previously (24).

Lipid Extraction—Serial dilutions of broth cultures cultivated in rifampin-free media were plated onto 7H10 plates supplemented with oleic acid-albumin-dextrose-catalase and 0.5% glycerol to obtain a confluent lawn in 21 days. Cells were scraped into a methanol-chloroform suspension (2:1) for sterilization and lipid extraction with Optima HPLC-grade solvents (Fisher) and clean disposable borosilicate glassware (Fisher, Supelco) with Teflon-lined caps as described previously (20) and dried with the GeneVac EZ-2 (SP Scientific) using the low boiling point mixture setting. Dried lipids were resuspended in chloroform and methanol (1:1, v/v), dried, and weighed (Mettler Toledo microbalance) prior to being resuspended in chloroform and methanol at 1 mg/ml. For quality control and to confirm normalization, 150 μg of cell wall lipids was spotted onto a silica thin-layer chromatography plate, developed with 60:35:5 (v/v/v, chloroform:methanol:water), and visualized with cupric acetate and charring. Mass normalization was further confirmed by comparative analysis of total ion current traces from lipid mixtures, ion monitoring of phosphatidylinositol, and continuous infusion of calibrants monitored at *m/z* 121.050873 and 922.009798 in positive ion mode and *m/z* 112.985587 and 1033.98810 in negative ion mode.

HPLC-ESI-Mass Quadrupole TOF Mass Spectrometry—We dried 100 μg of lipid extract under nitrogen and resuspended it at 0.5 mg/ml in solvent A (hexanes:isopropanol 70:30 (v/v), 0.02% (m/v) formic acid, 0.01% (m/v) ammonium hydroxide), filtered or centrifuged it at 1500 rpm for 5 min, and inspected it to assure lack of precipitation prior to transfer to a glass autosampler vial (Agilent) for analysis using an Agilent 6520 accurate mass quadrupole TOF and a 1200 series HPLC system with a Varian Monochrom diol column (3 μm $\times$ 150 mm $\times$ 2 mm) and a Varian Monochrom diol guard column (3 μm $\times$ 4.6 mm). 10 μg of lipid/sample was injected, and the column was eluted at 0.15 ml/min with a binary gradient from 0–100% solvent B (isopropanol:methanol 70:30 (v/v), 0.02% (m/v) formic acid, 0.01% (m/v) ammonium hydroxide): 0–10 min, 0% B; 17–22 min, 50% B; 30–35 min, 100% B; and 40–44 min, 0% B, followed by an additional 6-min 0% B post-run. Optimized conditions of 325 °C with a 5 liter/min countercurrent gas flow, a 30 pounds per square inch (psig) nebulizer pressure, and 5500 V were used (20). Spectra were collected in positive and negative ion mode from *m/z* 100–3000 at 1 spectrum/s. This method offers 10,000-fold dynamic range of intensity detection with a nearly linear relationship between input lipid mass signal intensity for diverse benchmark lipids over more than 1000-fold concentration range (20). CID-MS was carried out with energy of 30–60 V.

HPLC-MS Data Extraction—Raw data files were converted to mzData using MassHunter and processed in R software using XCMS (version 1.24) (25) and the centWave peak finder method (26). Briefly, peaks were deconvoluted and aligned across samples using signal-to-noise ratio threshold of 5, a maximum tolerated *m/z* deviation of 10 ppm, a frame width of *mzdiff* = 0.001, a peak width of 20–120 s, and a bandwidth of 5. The aligned output consisted of accurate mass, retention time, and intensity of each peak, exported as .tsv files or Microsoft Excel files for automatic annotation for compound matching within 10 ppm of the calculated mass (20). Automated annotation was confirmed based on retention times, accurate mass,

and detection of the naturally occurring length and saturation variants documented in the MycoMap database. XCMS data matrices allowed pairwise comparison using paired Student's *t* test with multiple testing correction (27).

Results

Growth Rates of Mycobacterial rpoB Mutants—We generated mutants using two genetically distinct strains that were originally derived from patients and now serve as reference strains: the lineage 4 or Euro-American strain known as CDC1551 and the lineage 2 or W-Beijing strain HN878. From larger panels of isogenic mutants in each strain background, we selected mutants corresponding to amino acid substitution at positions 526, 531, and 513 in the *rpoB* gene. We focused on three mutations, H526Y, S531L, and Q513E, because we had identified them in both genetic backgrounds and because they correspond to the characteristic mutations occurring among clinical isolates during natural tuberculosis epidemics (28, 29). As expected from prior reports, the S531L and H526Y mutations had a minimal effect on bacterial growth compared with wild-type organisms, whereas the Q513E mutation had a small but detectable effect on fitness (Fig. 1*A*).

Organism-wide Lipidomic Detection—An altered RNA polymerase might affect the expression of nearly any gene. However, where global profiling has been used, there is poor concordance between changes in transcript abundance and protein or small molecule abundance, presumably as a consequence of layers of posttranscriptional regulation. We therefore used an organism-wide profiling method to globally measure changes in mycobacterial cell wall lipids. Although most lipidomic or metabolomic methods focus on phospholipids, which constitute the bilayers of model eukaryotic cells and most bacteria, mycobacteria produce fewer phospholipids and more types of neutral lipids, including more than 90 subclasses of lipids that are unique to the order Actinomycetales (20, 23). Thus, mycobacterial lipid profiling relies mainly on positive ion mode monitoring and has been enabled by specific ionization methods for neutral lipids of high mass that form adducts with cations. New databases describe order- or genus-specific mycobacterial lipids (19, 20, 23). Our normal phase HPLC-MS system separates lipid classes covering the extremes of polarity, from apolar triacylglyerides and polyketides to phosphoglycolipids. Chromatographic preparation limits molecular heterogeneity at the electrospray interface at any moment in time, reducing cross-suppression, and retention time data facilitate compound naming using the MycoMass database (20). The ion chromatograms from one lipidomic profile illustrates ~12,000 distinct accurate mass retention time values detected and that individual overlaid chromatograms that correspond to compounds with unique accurate mass retention time values are distributed throughout the 42-min run (data not shown). The high dynamic range of TOF-MS allows detection of ions with an intensity from 2×10^2 to 6×10^6 counts, allowing parallel detection of abundant structural and trace lipids in one experiment (20).

The Comparative Lipidomics Data Analysis Pipeline—Each ion is reported as a molecular event, which is defined as one linked *m/z*, retention, and intensity value that is reported with mean intensity and variance. Among total detected events, artifacts derived from ions present in solvent blanks or ions

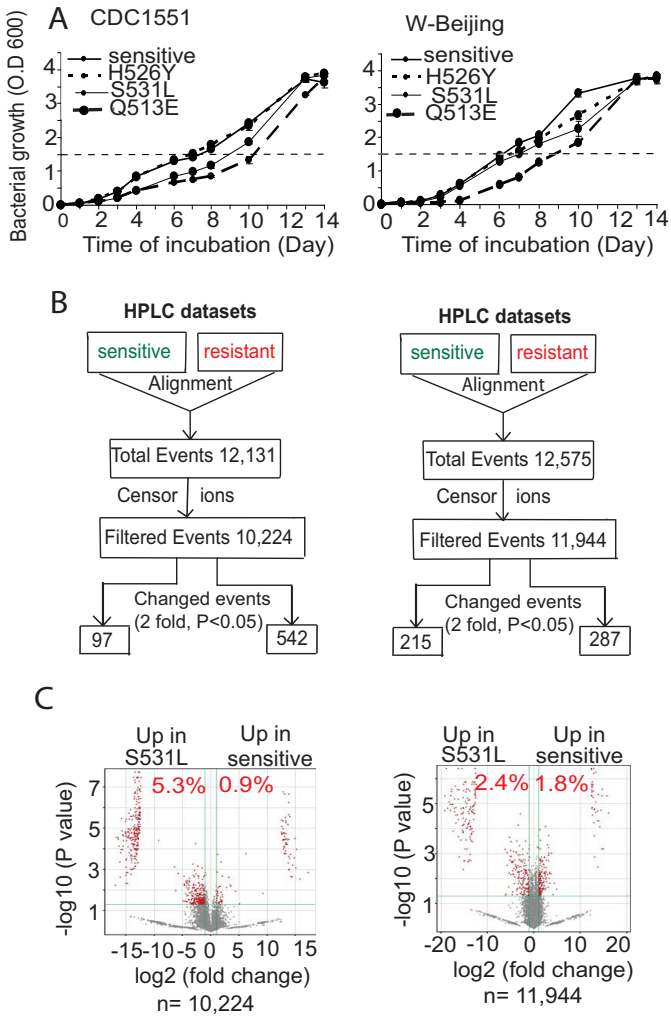

FIGURE 1. **Lipidomics data pipeline.** *A*, drug-sensitive (*sensitive*) parental and RpoB mutant strains identified according to the position of mutation (H526Y, S531L, and Q513E) were grown in antibiotic-free liquid medium. *O.D.*, optical density. *B*, triplicate lipidomic analysis of the drug-sensitive S531L mutant in the CDC1551 (*left panel*) and W-Beijing (*right panel*) backgrounds shows the total number of detected events. After excluding events that are also detectable in solvent blanks or not seen in all three HPLC runs, the list of "filtered events" more closely approximates the mycobacterial lipid profile. *C*, after aligning filtered events with equivalent mass and retention time values, paired values were assigned as intensity ratios (*dots*). Paired events with -fold change values of >2 with corrected $p < 0.05$ are considered to be biologically significant (*red dots*). The number of changed events divided by the number of filtered events gives a global value of lipid change (*red*).

detected in fewer than two replicates were censored to give a list of filtered events, ~10,000 per bacterium (Fig. 1*B*). Datasets from matched pairs of drug-resistant and drug-sensitive bacteria are aligned so that the intensity values of events with equivalent mass and retention time are considered to be the same molecule (Fig. 1*C*), and their intensity values are reported as ratios. An event is considered to be changed in the drug-resistant strain when intensity values differ by more than 2-fold with a corrected $p < 0.05$ (Fig. 1*B*) from the value corresponding to the drug-sensitive parental strain. The number of changed events is expressed as a percentage of all filtered events to yield a percent change value for the genetically altered bacterium, which is a quantitative description of the breadth of change of the lipid repertoire of the organism associated with acquisition

of the rifampin resistance mutation (Fig. 1*B*). Because each changed event is linked to accurate mass and retention time data, comparative lipidomics also provides a list of the changed molecules as defined by mass and retention time (supplemental Figs. S1 and S2). The chemical names of these molecules are then identified using their *m/z* value matches in databases (MycoMass, MycoMap) (20) or manual methods of collision-induced dissociation (CID) MS.

An S531L Mutation of rpoB Is Associated with Lipid Remodeling—To illustrate how this data pipeline is applied to identify patterns of rifampin resistance-associated changes in lipids, stepwise analysis of the rifampin-sensitive CDC1551 strain and its paired resistance mutant S531L is shown in a stepwise manner (Fig. 1, *B* and *C*). The two datasets yielded 12,131 total events of which 10,224 passed quality filters. Pairwise alignment of triplicate ion intensity values identify the subset of changed events that changed by more than 2-fold in intensity with significance (corrected $p < 0.05$), yielding 542 events up-regulated in the resistance mutant and 97 down-regulated (Fig. 1*B*).

In the normal phase, retention time correlates directly with chemical polarity. Prior analysis of benchmark lipids and the MycoMap dataset shows that lipids of low (triacylglycerol, PDIM), intermediate (sulfolipids, phospholipids) and high (high-order phosphoglycolipids) appear with early, intermediate, and late retention times, respectively. Different lipid classes have differing retention times, but alkyl form variants with altered saturation or chain length within each class nearly co-elute in the normal phase. Thus, alkyl forms are not distinguished based on retention time but can be recognized based on their *m/z* values (supplemental Figs. S1 and S2). When comparing S531L to its parental CDC1551 strain, we observed many changed events at diverse *m/z* values and retention times in all six mutants.

Display of all events as a volcano plot illustrates that events self-segregate into at least six definable clusters (Fig. 1*C*). The two clusters located at $>2^{10}$-fold-change are typically molecules that are not detected under one condition only. (These events have non-infinite -fold change values because low but detectable background values are present in all mass spectrometry measurements.) These lipids, which represent lipids detected in only one of the two bacteria, are potentially valuable as biomarkers of resistance or to identify specific lipid pathways altered because of their all-or-nothing expression state. Other lipids are present in both bacteria and typically show –fold change values of $<2^{10}$. These lipids are divided into color-coded clusters according to whether they do (red) or do not (gray) meet -fold change criteria, and the up- or down-regulated nature of the change associated with drug resistance is indicated by the leftward or rightward change from the midline. Finally, changed events are expressed as a percentage of filtered events, providing a total lipidic change score of 6.2% after S531L mutation in the CDC1551 strain (Fig. 1*C*). Thus, analysis of the first mutant detects a durable and broad remodeling of the lipid content of *M. tuberculosis* that is well above background changes because of variance in bacterial culture measured in prior experiments (0.7%) (20).

Lipidomic Phenotypes across the Rifampin Binding Site—To determine whether this rate of change was characteristic of rifampin-induced rpoB mutations, we carried out this analysis

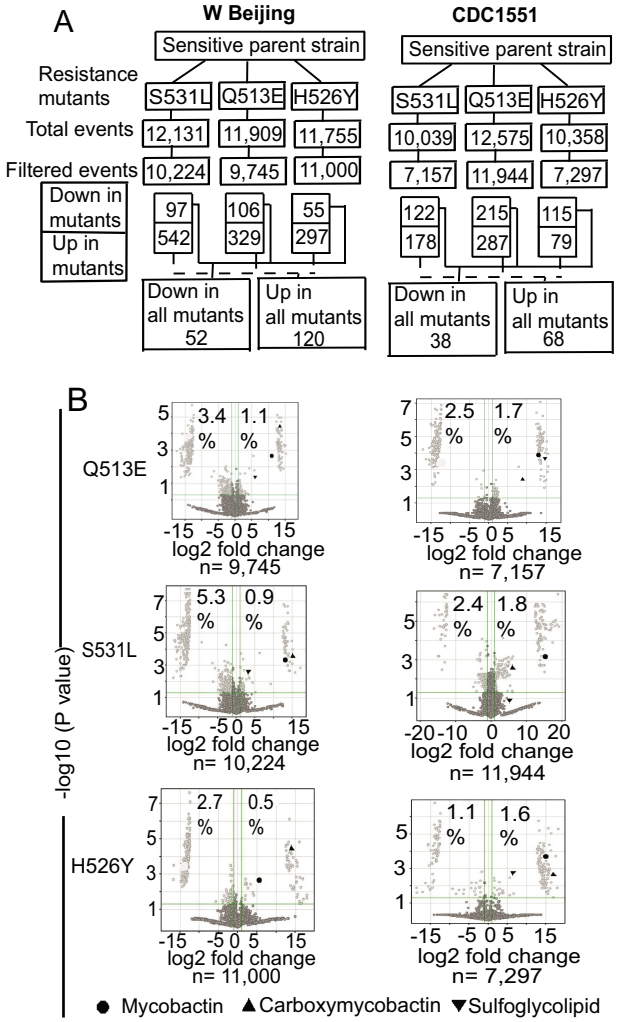

FIGURE 2. **Identification of globally changed events.** *A*, lists of all changed events for each of three mutants were compared to identify the subset of events changed in every mutant within each strain background. *B*, using mass values and the MycoMass database to preliminarily identify events corresponding to sulfoglycolipid, mycobactin, and carboxymycobactin, named (*black*) and unnamed unchanged (*gray*) events are shown.

for each of the six rifampin resistance mutants, which covers three sites in each of two genetic backgrounds. Pairwise comparison of drug-sensitive and -resistant strains altered at three positions (S531L, Q513E, and H526Y) showed a similar percentage change in all point mutants in both the CDC1551 and W-Beijing backgrounds (Fig. 2), ranging from 2.7–6.2%. The hundreds of changed events present in any mutant exceeded the practical capacity to identify them. To prioritize lipid targets with the highest penetrance, we carried out a meta-analysis to identify individual events present in most or all of the mutants. Using computer-generated lists of changed events derived from each point mutant, we manually compared the changed ions common to all mutants in each strain to identify globally changed events (Fig. 2*A*). This analysis yielded 172 events for W-Beijing (supplemental Fig. S1) and 106 events for CDC1551 (supplemental Fig. S2). The capture of large numbers of events that were durably changed among all three mutants in both strains validated the reproducibility of new organism-wide detection methods. The existence of globally changed events rep-

resented evidence for the existence of stereotyped biochemical changes in *M. tuberculosis* in response to rifampin resistance that are independent of the particular residue mutated.

Mass-based Identification of Named Lipids—Next we sought to identify the molecules corresponding to globally changed events, taking advantage of the fact that each changed event is linked to accurate mass-retention time data. R software compared the 278 globally changed events (supplemental Figs. S1 and S2) to ~30,000 collected mass values of mycobacterial lipids in the MycoMass database (20) within 10 ppm error. For CDC1551 mutants, software annotation matched five globally changed events to mass values of ferrimycobactin ($[M+Fe-2H]^+$ = 909.455) or ferricarboxymycobactins ($[M+Fe-2H]^+$ = 785.2577, 799.274, 815.304, 841.321, 909.455). Five events matched diacylated sulfoglycolipid ($[M+H]^+$ = *m/z* 1296.9632, 1364.0284, 1381.0551, 1395.0691, and 149.80622). In all cases, the ions corresponding to these lipids were down-regulated in drug resistance mutants (supplemental Fig. S1). Analysis of W-Beijing identified 10 globally altered events, with eight matching the expected masses of ferricarboxymycobactins and two matching mycobactins. In all cases, signals were down-regulated in the resistance mutant. Although events matching sulfolipid were not seen in the list of ions meeting change criteria in all three CDC1551 mutants, their identification as globally changed events in all three W-Beijings prompted a manual reanalysis. We found a reduced sulfoglycolipid signal in the mutant in all three cases, although the reduction did not reach statistical significance in the S531L mutant. Overall, sulfoglycolipid signals were reduced in all six tested strains, reaching significance in five of six cases.

Overview of Automated Lipidomics Results—These targets were identified using a semiautomated analysis of more than 1 million data points of a newly developed discovery platform. Several aspects of the pattern suggested that the organism-wide method was reliable and that mycobactins, carboxymycobactins, and sulfoglycolipids likely constituted characteristic features of the *rpoB* mutation response. First, among more than 109 subclasses of lipids detected, these three classes of named lipids showed statistically changed intensity values among all mutants, or all but one mutant, in both genetic backgrounds. Second, in all cases, the direction of change was the same. Third, in most cases, the automated analysis independently identified several molecular variants corresponding to an alkane series changing in parallel with the same direction and similar magnitude (supplemental Figs. S1 and S2). These lipids were of biological interest because they have known roles in virulence (30–33), growth (21), or provoking the human immune response in the CD1 system (21, 34, 35). Also, all three types of lipids are produced at moderately high concentrations and are easily detected with standard analytical techniques and so would be candidate biomarkers for developing clinical tests for the drug-resistant state. However, these targets were identified with newly developed tools used in high throughput in a screening mode. Therefore, we next sought to validate the semiautomated methods using manual analysis of two standard analytical chemistry approaches: ion chromatograms and CID-MS (Fig. 3 and supplemental Fig. S3).

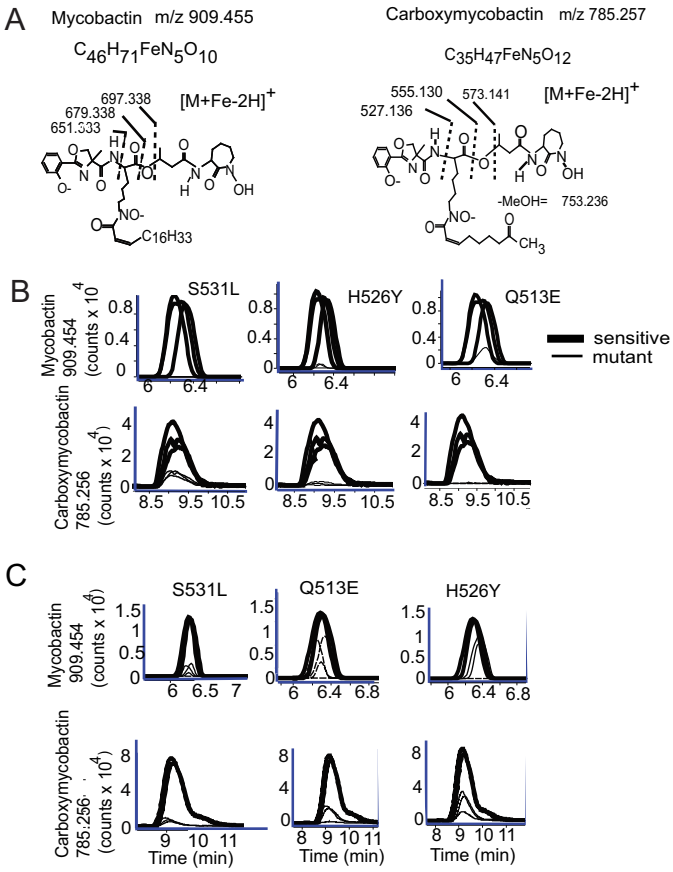

FIGURE 3. **Validation of automated detection of mycobactins using analytical chemistry methods.** *A*, focusing on ions whose detected *m/z* values match the theoretical values for ferrimycobactin and ferricarboxymycobactin [M+Fe-2H] within experimental error, positive mode CID-MS generated the indicated fragment ions. *B* and *C*, software-derived intensity values using XCMS curve fitting software shown in Fig. 2 were validated using raw data generated as ion chromatograms corresponding to the known masses of mycobactin (909.4) and carboxymycobactin (785.3). *B*, W-Beijing. *C*, CDC1551.

Validation of Automated Lipidomics Methods—Manual analyses of total ion current and the ions corresponding to two abundant lipids that served as loading controls (phosphatidylethanolamine and cardiolipin) confirmed that the total input lipid from the parental and mutant strains was similar (supplemental Fig. S4 *A*). Next, CID-MS of events corresponding to the known mass of ferrimycobactin (supplemental Fig. S3) provided spectra that ruled in the detected molecules as mycobactins. For example, CID-MS of $[M+Fe-2H]^+$ ions (*m/z* 909.456) detected the diagnostic mycobactin (*m/z* 679.338, *m/z* 697.338), cobactin, as well as other characteristic fragments that matched the deduced structure (Fig. 3*A* and supplemental Fig. S3*A*) (21). Also, manually generated ion chromatograms showed maxima that matched the observed retention time of 6.3 min for ferrimycobactin in the MycoMap database (Fig. 3*B*) (20). Manually generated ion chromatograms from drug-sensitive and -resistant bacteria confirmed the marked or complete loss of signals corresponding to the mass of a proton adduct of ferrimycobactin in all drug-resistant mutants in both the CDC1551 (Fig. 3*B*) and W-Beijing (Fig. 3*C*) backgrounds. The patterns seen in the most abundant ferrimycobactin (*m/z* 909.456) were recapitulated in ion chromatograms of natural variants that differed by a single saturation (*m/z* 911.470) or alkyl chain unit (*m/z*

923.470) (supplemental Fig. S4). Although intensity values measured in a screening mode do not establish the absolute concentrations of these lipids, prior analyses of sulfolipids and mycobactins validate a nearly linear response of mass input to MS signal intensity within the intensity ranges measured here (20). Overall, both automated and manual analyses were in good agreement and indicated a marked reduction of mycobactin siderophore biosynthesis by rifampin-resistant mutants as a percentage of the mass of all lipids produced.

Using the same approach, we confirmed that the globally changed events initially assigned as ferricarboxymycobactin (*m/z* 785.257) corresponded to authentic carboxymycobactins. This conclusion was supported by CID-MS experiments (Fig. 3*A*), and ion chromatograms showed retention times (9.1 min) that matched those of carboxymycobactins in the MycoMap database (20). A markedly reduced signal intensity corresponding to ferricarboxymycobactin (*m/z* 785.261) was observed for drug-resistant mutants in all cases (Fig. 3, *B* and *C*). Signals corresponding to natural alkane and saturation variants (*m/z* 773.256 and 813.288) also showed a marked reduction in resistance mutants as well (supplemental Fig. S4, *C* and *E*). In contrast to the complete loss of MS signals for mycobactin and carboxymycobactin seen with knockout of biosynthetic genes (21, 36), we observed less than complete suppression in all mutants for both siderophore types, an observation that was consistent with regulated suppression of siderophores by *M. tuberculosis* in the drug-resistant state.

RpoB Mutations Are Associated with a Reduction in Sulfoglycolipids—After automated analysis identified five late-eluting, globally changed molecular events as likely sulfoglycolipids (Fig. 2 and supplemental Figs. S1 and S2), conventional analysis with CID-MS in the positive mode assigned key fragments as ammonium adducts of diacylated sulfoglycolipids. For example, fragmentation of the parent ion *m/z* 1296.984 as $[M+NH4]^+$ yielded ions corresponding to the loss of dually dehydrated sulfoglucose (*m/z* 1019.9218), phthioceranic (*m/z* 573.592) and fatty acids (*m/z* 267.271, 239.241), as well as other expected fragments (Fig. 4*A* and supplemental Fig. S3*C*). Using positive mode ion scanning, the sulfoglycolipids were initially detected as ammonium adducts in the screening mode. Sulfolipids readily form anions $[M-H]^-$. Although the automated whole organism analysis emphasizes positive mode scanning for broader coverage, knowledge that sulfoglycolipid, which forms anions because of its sulfate moiety, led to a second, targeted analysis of negative mode ion chromatograms. This targeted approach, derived from the known ionization properties of sulfolipids, provided a high signal intensity corresponding to deprotonated diacyl SGLs (*m/z* 1277.927, [M-H]-, C70H133O17S), which showed a marked down-regulation of signals for diacylated sulfoglycolipid after RpoB mutation in five of six mutants (Figs. 2 and 4, *B* and *C*). For S531L in CDC1551, the mutant also showed a trend toward a lower SGL signal than the sensitive parent, but this effect was not statistically significant (Fig. 4*B*). Overall, new lipidomic scanning methods and conventional analysis of analytical chemistry provide clear evidence for the down-regulation of SGL intensity as a penetrant feature of rifampin-resistant mutants.

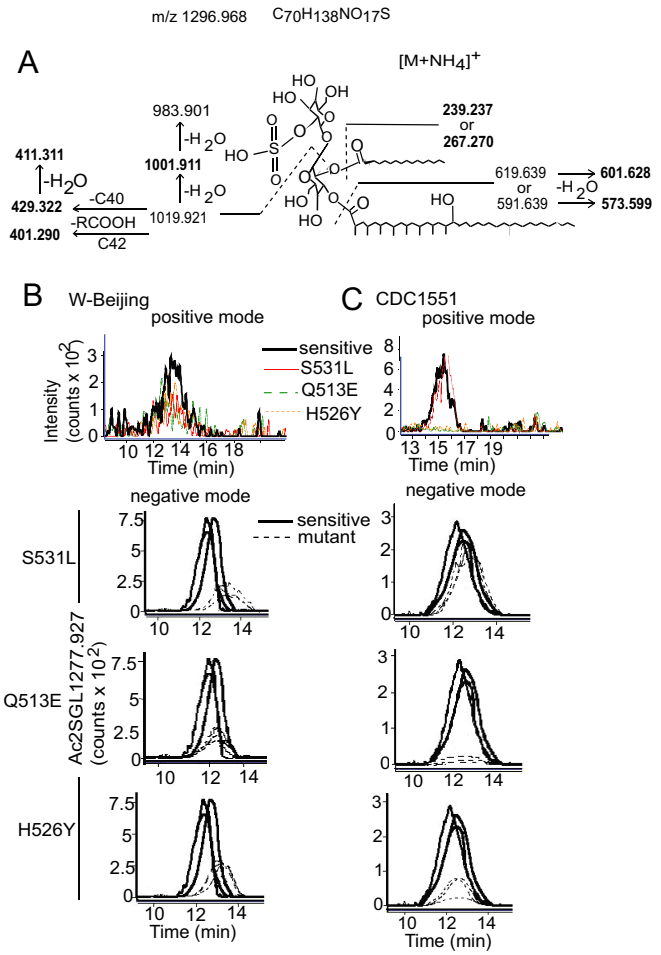

FIGURE 4. **Association of the *rpoB* mutation with sulfoglycolipid expression (Ac2SGL).** *A*, focusing on ions whose detected *m/z* values match the theoretical values for Ac2SGL $[M+NH4^+]^+$, CID-MS, detecting the indicated fragment ions corresponding to the loss of hexose sulfate, fatty acyl units, and the indicated phthioceranic acid. *B* and *C*, to validate intensity values generated using curve fitting software, ion chromatograms corresponding to the known masses of AC2SGL (*m/z* 1277.9) were generated manually.

Targeted Reanalysis of Known Lipids—The central goal of this work was the use of unbiased methods to discover new lipid markers with high penetrance. However, previously reported lipid changes can also be evaluated with these datasets. Previously, little was known about changes in lipids associated with *rpoB* mutations, but Bisson *et al.* (13) identified changes in peptides from PDIM biosynthetic genes using proteomic methods. Whether or not the PDIM end product of this pathway also changed could not be unequivocally determined, but this work did document increases in the intensity of certain ions corresponding to PDIM fragments and an increase in PDIM ions in one mutant studied. Therefore, to ask the targeted question about PDIM abundance in our mutants, we deduced the mass of PDIM (*m/z* 1371.4) fragments in the positive mode, identified ions matching this mass, and confirmed their identify as PDIM using CID-MS (supplemental Fig. S5*A*). Subsequently we found increases in PDIM signals for three PDIM chain length analogs in three of three mutants in the W-Beijing background (supplemental Fig. S5, *B* and *C*) but not in all mutants of the CDC1551 background (data not shown). However, the PDIM molecules did not feature in the list of up-regulated ions

in supplemental Fig. S1 as the changes in signal did not meet the stringent criteria for high -fold change and low p values (supplemental Fig. S5*B*). These results suggest that PDIM changes are not as broadly seen in resistance mutants as compared with lipid changes discussed above. However, the data are consistent with the conclusion that PDIM concentrations can be increased in rifampin-resistant strains. Although the prior report found changes in phosphatidylglycerol using methods different from those used here, we did not see significant or penetrant changes in the phosphatidylglycerol signal.

Discussion

Genetic changes in the rifampin binding site render Gram-negative and mycobacteria genetically resistant to rifampin and represent the primary genetic mechanism of drug resistance, accounting for nearly all clinically important cases of rifampin resistance (28, 37). Molecules that are reproducibly changed after the evolution of the drug-resistant state are candidates for development as biomarkers of the resistant state or might point toward biological pathways involved in secondary, non-genetic mechanisms of phenotypic resistance to drugs (9, 38–41). Mycobacteria produce an unusually complex cell envelope composed of phospholipid, mycolyl lipid, and other layers that are actively regulated and remodeled as part of the switch to dormancy or in response to metabolic stresses (19). Therefore, we considered it plausible that organism-wide alterations in cell wall lipids might arise after genetic acquisition of rifampin resistance. Here we focused on mutations in RpoB at amino acid positions 513, 526, and 531, which are mutated under drug selection in clinical isolates. Both the scope and the identity of the changed lipids show reproducible patterns present in all tested mutants, regardless of the specific amino acid position. Three lipid classes, mycobactins, carboxymycobactins, and sulfoglycolipids, show significant changes in signal strength within any single mutant and among independent residues near the rifampin binding site (20), in two genetic backgrounds. These data support the view that RpoB mutations that inactivate rifampin binding cause durable genetic changes that broadly and reproducibly influence *M. tuberculosis* lipid content.

The scope of change was similar among all mutants, ranging from 2.7–6.2% of detectable lipids. Recent studies that measured global lipidic change under experimentally defined conditions provide a context for interpreting whether this represents a low or high degree of lipid remodeling. Variance in lipid profiles derived from growing bacteria in biological triplicate causes a false positive detection rate of 0.7%, with this low rate derived from the variance in density of bacteria during *in vitro* growth in medium. In contrast, the rates of change measured here for RpoB mutants approximate 5% and are similar to total lipid change values found when comparing two evolutionary distinct strains, *M. tuberculosis* H37Rv and W-Beijing (20). Because the total changes seen among strains with mutations in a single gene approximate the degree of lipid change that characterizes separately evolved *M. tuberculosis* strains that are well recognized as distinct, we interpret *rpoB* mutation as inducing a high rate of lipidic change in *M. tuberculosis*.

This new lipidomics platform identified the most characteristic features of the rifampin resistant phenotype, supporting long-term efforts to understand the evolution of multidrug-resistant tuberculosis and validate chemical markers of the resistant state. Several aspects of these data indicate that changes in mycobactin, carboxymycobactin, and sulfoglycolipid are likely characteristic of rifampin binding site mutations. In nearly all cases, the lipid classes identified as changed from semiautomated, organism-wide screens of molecular events were in agreement with those seen in targeted analyses with more detailed analytical biochemical methods. The only clear area of divergence in outcomes measured by manual and automated methods was that sulfoglycolipid showed stronger and more reproducible changes in the manually generated chromatogram in the negative mode compared with positive mode scanning. This finding provides a rationale for positive and negative mode lipidomic scanning in the future and illustrates the usefulness of targeted follow-up experiments completed after the whole organism screen identifies candidate targets. Overall, the agreement of automated and manual methods further validated key aspects of the newly developed lipidomics platform as a discovery tool in a biological context.

Finally, the reproducible nature of the changed molecules among replicates, mutation sites, and strain backgrounds supports future studies into altered biochemical physiology of *rboB* mutant bacteria. Mycobactin and carboxymycobactin function coordinately as a system for uptake of iron from extracellular stores into the cytosol, which is essential for mycobacterial growth (21, 31, 42). To our knowledge, the binding of ferric iron binding to the IdeR and the resulting suppression of mycobactin synthase transcription is the only known mechanism for coordinated suppression of this iron uptake pathway (43, 44). These experiments, conducted in iron-replete medium, imply that rifampin-resistant mycobacteria likely have either altered iron sensing or iron or undiscovered interactions with the IdeR pathway. Sulfoglycolipids represent abundant polyketides with known or proposed roles in promoting virulence (30, 33, 45, 46) or the host immune response (35). Both lipids localize to the outer cell wall through complex, multistep export pathways that involve MmpL transporters. Both their abundance and surface localization have suggested possible roles in direct interface with host membranes or alterations in cell wall permeability. Thus, the discovery of reproducibly altered polyketide lipid biosynthesis in rifampin resistance mutants points toward a specific candidate mechanism of altered cell wall permeability or virulence that can be tested in future studies of infected animals and drug permeability of rifampin-resistant organisms.

Author Contributions—N. L. performed the lipidomics experiments and data analysis and contributed to writing the manuscript. R. R. S., C. F., and S. M. F. designed, generated, and characterized the rifampin resistance mutants. E. L. and D. Y. conducted the analytical chemistry and CID-MS experiments. D. B. M., M. B. M., and S. M. F. devised the concept and wrote the manuscript. D. B. M. provided project oversight.

References

1. Koul, A., Arnoult, E., Lounis, N., Guillemont, J., and Andries, K. (2011) The challenge of new drug discovery for tuberculosis. *Nature* **469,** 483–490

2. Keshavjee, S., and Farmer, P. E. (2012) Tuberculosis, drug resistance, and the history of modern medicine. *N. Engl. J. Med.* **367,** 931–936
3. Velayati, A. A., Farnia, P., Mozafari, M., Sheikholeslami, M. F., Karahrudi, M. A., Tabarsi, P., and Hoffner, S. (2014) High prevalence of rifampin-monoresistant tuberculosis: a retrospective analysis among Iranian pulmonary tuberculosis patients. *Am. J. Trop Med. Hyg.* **90,** 99–105
4. Coovadia, Y. M., Mahomed, S., Pillay, M., Werner, L., and Mlisana, K. (2013) Rifampicin mono-resistance in *Mycobacterium tuberculosis* in KwaZulu-Natal, South Africa: a significant phenomenon in a high prevalence TB-HIV region. *PLoS ONE* **8,** e77712
5. Franke, M. F., Appleton, S. C., Mitnick, C. D., Furin, J. J., Bayona, J., Chalco, K., Shin, S., Murray, M., and Becerra, M. C. (2013) Aggressive regimens for multidrug-resistant tuberculosis reduce recurrence. *Clin. Infect. Dis.* **56,** 770–776
6. Cummings, M. P., and Segal, M. R. (2004) Few amino acid positions in rpoB are associated with most of the rifampin resistance in *Mycobacterium tuberculosis*. *BMC Bioinformatics* **5,** 137
7. Goldstein, B. P. (2014) Resistance to rifampicin: a review. *J. Antibiot.* **67,** 625–630
8. Boehme, C. C., Nabeta, P., Hillemann, D., Nicol, M. P., Shenai, S., Krapp, F., Allen, J., Tahirli, R., Blakemore, R., Rustomjee, R., Milovic, A., Jones, M., O'Brien, S. M., Persing, D. H., Ruesch-Gerdes, S., *et al.* (2010) Rapid molecular detection of tuberculosis and rifampin resistance. *N. Engl. J. Med.* **363,** 1005–1015
9. Comas, I., Borrell, S., Roetzer, A., Rose, G., Malla, B., Kato-Maeda, M., Galagan, J., Niemann, S., and Gagneux, S. (2012) Whole-genome sequencing of rifampicin-resistant *Mycobacterium tuberculosis* strains identifies compensatory mutations in RNA polymerase genes. *Nat. Genet.* **44,** 106–110
10. Ezekiel, D. H., and Hutchins, J. E. (1968) Mutations affecting RNA polymerase associated with rifampicin resistance in *Escherichia coli*. *Nature* **220,** 276–277
11. Tocchini-Valentini, G. P., Marino, P., and Colvill, A. J. (1968) Mutant of *E. coli* containing an altered DNA-dependent RNA polymerase. *Nature* **220,** 275–276
12. de Knegt, G. J., Bruning, O., ten Kate, M. T., de Jong, M., van Belkum, A., Endtz, H. P., Breit, T. M., Bakker-Woudenberg, I. A., and de Steenwinkel, J. E. (2013) Rifampicin-induced transcriptome response in rifampicin-resistant *Mycobacterium tuberculosis*. *Tuberculosis* **93,** 96–101
13. Bisson, G. P., Mehaffy, C., Broeckling, C., Prenni, J., Rifat, D., Lun, D. S., Burgos, M., Weissman, D., Karakousis, P. C., and Dobos, K. (2012) Up-regulation of the phthiocerol dimycocerosate biosynthetic pathway by rifampin-resistant, rpoB mutant *Mycobacterium tuberculosis*. *J. Bacteriol.* **194,** 6441–6452
14. Cambier, C. J., Takaki, K. K., Larson, R. P., Hernandez, R. E., Tobin, D. M., Urdahl, K. B., Cosma, C. L., and Ramakrishnan, L. (2014) Mycobacteria manipulate macrophage recruitment through coordinated use of membrane lipids. *Nature* **505,** 218–222
15. Camacho, L. R., Constant, P., Raynaud, C., Laneelle, M. A., Triccas, J. A., Gicquel, B., Daffe, M., and Guilhot, C. (2001) Analysis of the phthiocerol dimycocerosate locus of *Mycobacterium tuberculosis*: evidence that this lipid is involved in the cell wall permeability barrier. *J. Biol. Chem.* **276,** 19845–19854
16. Favrot, L., and Ronning, D. R. (2012) Targeting the mycobacterial envelope for tuberculosis drug development. *Expert Rev. Anti Infect. Ther.* **10,** 1023–1036
17. Pang, J. M., Layre, E., Sweet, L., Sherrid, A., Moody, D. B., Ojha, A., and Sherman, D. R. (2012) The polyketide Pks1 contributes to biofilm formation in *Mycobacterium tuberculosis*. *J. Bacteriol.* **194,** 715–721
18. Minnikin, D. E., Kremer, L., Dover, L. G., and Besra, G. S. (2002) The methyl-branched fortifications of *Mycobacterium tuberculosis*. *Chem. Biol.* **9,** 545–553
19. Layre, E., and Moody, D. B. (2013) Lipidomic profiling of model organisms and the world's major pathogens. *Biochimie* **95,** 109–115
20. Layre, E., Sweet, L., Hong, S., Madigan, C. A., Desjardins, D., Young, D. C., Cheng, T. Y., Annand, J. W., Kim, K., Shamputa, I. C., McConnell, M. J., Debono, C. A., Behar, S. M., Minnaard, A. J., Murray, M., *et al.* (2011) A comparative lipidomics platform for chemotaxonomic analysis of *Mycobacterium tuberculosis*. *Chem. Biol.* **18,** 1537–1549
21. Madigan, C. A., Cheng, T. Y., Layre, E., Young, D. C., McConnell, M. J., Debono, C. A., Murry, J. P., Wei, J. R., Barry, C. E., 3rd, Rodriguez, G. M., Matsunaga, I., Rubin, E. J., and Moody, D. B. (2012) Lipidomic discovery of deoxysiderophores reveals a revised mycobactin biosynthesis pathway in *Mycobacterium tuberculosis*. *Proc. Natl. Acad. Sci. U.S.A.* **109,** 1257–1262
22. Galagan, J. E., Minch, K., Peterson, M., Lyubetskaya, A., Azizi, E., Sweet, L., Gomes, A., Rustad, T., Dolganov, G., Glotova, I., Abeel, T., Mahwinney, C., Kennedy, A. D., Allard, R., Brabant, W., *et al.* (2013) The *Mycobacterium tuberculosis* regulatory network and the hypoxic response. *Nature* **499,** 178–183
23. Sartain, M. J., Dick, D. L., Rithner, C. D., Crick, D. C., and Belisle, J. T. (2011) Lipidomic analyses of *Mycobacterium tuberculosis* based on accurate mass measurements and the novel "Mtb LipidDB." *J. Lipid Res.* **52,** 861–872
24. Ford, C. B., Shah, R. R., Maeda, M. K., Gagneux, S., Murray, M. B., Cohen, T., Johnston, J. C., Gardy, J., Lipsitch, M., and Fortune, S. M. (2013) *Mycobacterium tuberculosis* mutation rate estimates from different lineages predict substantial differences in the emergence of drug-resistant tuberculosis. *Nat. Genet.* **45,** 784–790
25. Smith, C. A., Want, E. J., O'Maille, G., Abagyan, R., and Siuzdak, G. (2006) XCMS: processing mass spectrometry data for metabolite profiling using nonlinear peak alignment, matching, and identification. *Anal. Chem.* **78,** 779–787
26. Tautenhahn, R., Böttcher, C., and Neumann, S. (2008) Highly sensitive feature detection for high resolution LC/MS. *BMC Bioinformatics* **9,** 504
27. Benjamini, Y., and Hocheberg, Y. (1995) Controlling the false discovery rate: a practical and powerful approach to multiple testing. *J. R. Stat. Soc.* **57,** 289–300
28. Campbell, E. A., Korzheva, N., Mustaev, A., Murakami, K., Nair, S., Goldfarb, A., and Darst, S. A. (2001) Structural mechanism for rifampicin inhibition of bacterial RNA polymerase. *Cell* **104,** 901–912
29. Campbell, P. J., Morlock, G. P., Sikes, R. D., Dalton, T. L., Metchock, B., Starks, A. M., Hooks, D. P., Cowan, L. S., Plikaytis, B. B., and Posey, J. E. (2011) Molecular detection of mutations associated with first- and second-line drug resistance compared with conventional drug susceptibility testing of *Mycobacterium tuberculosis*. *Antimicrob. Agents Chemother.* **55,** 2032–2041
30. Converse, S. E., Mougous, J. D., Leavell, M. D., Leary, J. A., Bertozzi, C. R., and Cox, J. S. (2003) MmpL8 is required for sulfolipid-1 biosynthesis and *Mycobacterium tuberculosis* virulence. *Proc. Natl. Acad. Sci. U.S.A.* **100,** 6121–6126
31. De Voss, J. J., Rutter, K., Schroeder, B. G., Su, H., Zhu, Y., Barry, C. E., 3rd (2000) The salicylate-derived mycobactin siderophores of *Mycobacterium tuberculosis* are essential for growth in macrophages. *Proc. Natl. Acad. Sci. U.S.A.* **97,** 1252–1257
32. Seeliger, J. C., Holsclaw, C. M., Schelle, M. W., Botyanszki, Z., Gilmore, S. A., Tully, S. E., Niederweis, M., Cravatt, B. F., Leary, J. A., and Bertozzi, C. R. (2012) Elucidation and chemical modulation of sulfolipid-1 biosynthesis in *Mycobacterium tuberculosis*. *J. Biol. Chem.* **287,** 7990–8000
33. Gilmore, S. A., Schelle, M. W., Holsclaw, C. M., Leigh, C. D., Jain, M., Cox, J. S., Leary, J. A., and Bertozzi, C. R. (2012) Sulfolipid-1 biosynthesis restricts *Mycobacterium tuberculosis* growth in human macrophages. *ACS Chem. Biol.* **7,** 863–870
34. Moody, D. B., Young, D. C., Cheng, T. Y., Rosat, J. P., Roura-Mir, C., O'Connor, P. B., Zajonc, D. M., Walz, A., Miller, M. J., Levery, S. B., Wilson, I. A., Costello, C. E., and Brenner, M. B. (2004) T cell activation by lipopeptide antigens. *Science* **303,** 527–531
35. Gilleron, M., Stenger, S., Mazorra, Z., Wittke, F., Mariotti, S., Böhmer, G., Prandi, J., Mori, L., Puzo, G., and De Libero, G. (2004) Diacylated sulfoglycolipids are novel mycobacterial antigens stimulating CD1-restricted T Cells during infection with *Mycobacterium tuberculosis*. *J. Exp. Med.* **199,** 649–659
36. Madigan, C. A., Martinot, A. J., Wei, J. R., Madduri, A., Cheng, T. Y., Young, D. C., Layre, E., Murry, J. P., Rubin, E. J., and Moody, D. B. (2015) Lipidomic analysis links mycobactin synthase K to iron uptake and virulence in *M. tuberculosis*. *PLoS Pathog.* **11,** e1004792

37. Vassylyev, D. G., Vassylyeva, M. N., Zhang, J., Palangat, M., Artsimovitch, I., and Landick, R. (2007) Structural basis for substrate loading in bacterial RNA polymerase. *Nature* **448,** 163–168
38. de Vos, M., Müller, B., Borrell, S., Black, P. A., van Helden, P. D., Warren, R. M., Gagneux, S., and Victor, T. C. (2013) Putative compensatory mutations in the rpoC gene of rifampin-resistant *Mycobacterium tuberculosis* are associated with ongoing transmission. *Antimicrob. Agents Chemother.* **57,** 827–832
39. Brandis, G., Wrande, M., Liljas, L., and Hughes, D. (2012) Fitness-compensatory mutations in rifampicin-resistant RNA polymerase. *Mol. Microbiol.* **85,** 142–151
40. Strauss, O. J., Warren, R. M., Jordaan, A., Streicher, E. M., Hanekom, M., Falmer, A. A., Albert, H., Trollip, A., Hoosain, E., van Helden, P. D., and Victor, T. C. (2008) Spread of a low-fitness drug-resistant *Mycobacterium tuberculosis* strain in a setting of high human immunodeficiency virus prevalence. *J. Clin. Microbiol.* **46,** 1514–1516
41. Gagneux, S., Long, C. D., Small, P. M., Van, T., Schoolnik, G. K., and Bohannan, B. J. (2006) The competitive cost of antibiotic resistance in *Mycobacterium tuberculosis*. *Science* **312,** 1944–1946
42. Ratledge, C. (2004) Iron, mycobacteria and tuberculosis. *Tuberculosis* **84,** 110–130
43. Quadri, L. E., Sello, J., Keating, T. A., Weinreb, P. H., and Walsh, C. T. (1998) Identification of a *Mycobacterium tuberculosis* gene cluster encoding the biosynthetic enzymes for assembly of the virulence-conferring siderophore mycobactin. *Chem. Biol.* **5,** 631–645
44. Gold, B., Rodriguez, G. M., Marras, S. A., Pentecost, M., and Smith, I. (2001) The *Mycobacterium tuberculosis* IdeR is a dual functional regulator that controls transcription of genes involved in iron acquisition, iron storage and survival in macrophages. *Mol. Microbiol.* **42,** 851–865
45. Jain, M., Petzold, C. J., Schelle, M. W., Leavell, M. D., Mougous, J. D., Bertozzi, C. R., Leary, J. A., and Cox, J. S. (2007) Lipidomics reveals control of *Mycobacterium tuberculosis* virulence lipids via metabolic coupling. *Proc. Natl. Acad. Sci. U.S.A.* **104,** 5133–5138
46. Domenech, P., Reed, M. B., Dowd, C. S., Manca, C., Kaplan, G., and Barry, C. E., 3rd (2004) The role of MmpL8 in sulfatide biogenesis and virulence of *Mycobacterium tuberculosis*. *J. Biol. Chem.* **279,** 21257–21265